

1 **Abstract**

2 An intensive experimental investigation by means of triaxial and oedometer tests was
3 performed on a clayey loess that was retrieved from two depths at a location on the
4 southern Chinese Loess Plateau. Intact and reconstituted samples were used to identify
5 the effects of the natural structure on soil behavior in saturated conditions. The behavior
6 in compression was clearly affected by structure with the intact samples reaching well-
7 defined gross yield points outside the intrinsic compression line of the reconstituted soil,
8 after which the compression paths converged towards the intrinsic compression lines,
9 behavior which is consistent with destructuration. However, very high stresses were
10 required to give complete convergence. Similarly the triaxial tests that were carried out
11 at lower stress levels also did not give convergence of the critical states so that different
12 critical state lines could be defined for the intact and reconstituted soils. This was
13 consistent with qualitative observations from scanning electron micrographs that
14 natural elements of fabric and possibly bonding persisted even after triaxial shearing.
15 The effects of structure at the two depths on the compression and shearing behavior
16 were slightly larger for the shallower samples. Despite the very different genesis of the
17 soils, it was found that similar frameworks could be applied to those used for
18 sedimentary clays and that the degree of structure was equivalent to a clay of medium
19 sensitivity.

20

1 INTRODUCTION

2 During the Pleistocene, loess transported by wind was deposited widely in China
3 (Heller & Liu 1982; Kukla & An 1989). As a result of this genesis, the Aeolian soils
4 deposited under free-fall typically form highly open structures with the interstitial clay-
5 particles congregating at the silt-particles contacts. The finer particles and particle
6 aggregates have low settling velocities, and they were generally deposited further from
7 the source area. The finer particle content of loess on the Chinese Loess Plateau
8 increases from northwest to southeast (Fig.1). They are classified progressively as
9 sandy loess, silty loess and clayey loess (Liu, 1985). It is the clayey loess from Jingyang
10 on the southeast margins of the plateau (Fig.1), also investigated by Jiang et al. (2014),
11 which has been used here to identify in detail the influence of structure on its behavior.

12
13 Loess soils around the world are frequently partially saturated in-situ and much research
14 has focused on their collapse on wetting (e.g. Rogers et al., 1994; Muñoz-Castelblanco
15 et al., 2011; Jiang et al., 2012). The element of structure that is linked to that collapse
16 is typically thought to be inter-particle bonding, but researchers are not unanimous
17 about the origins of the inter-particle bonds. Some have emphasized clay particles, often
18 in aggregated form, linking larger silt grains (e.g. Barden et al., 1973; Delage et al.,
19 2005), but others refer to calcite bonding, dissolved salts or iron oxide (e.g. Derbyshire
20 et al., 1995; Jiang et al., 2012). While a loss of bonding may be the cause of the collapse,
21 its magnitude is related to the open fabric of the loess and many authors have used
22 Scanning Electron Microscopy, Mercury Intrusion Porosimetry or Computed

1 Tomography to investigate this (e.g. Delage et al., 2005; Wen & Yan, 2013; Jiang et al.,
2 2014).

3

4 There has been a significant amount of work examining the effects of structure on other
5 aspects of the behavior of partially saturated loess, not just collapse (e.g. Wen and Yan,
6 2013). While some researchers have suggested a more or less complete loss of bonding
7 on saturation (Dijkstra et al., 2000; Dijkstra, 2001), others have found significant effects
8 of structure even in the saturated soils (e.g. Feda et al., 1993; Jiang et al., 2014).

9 Reviewing existing data (Hu et al., 2004; Chen et al., 2006; Shao et al., 2006; Li & Yao,
10 2009), Liu et al. (2013) identified the similarity between the behavior of intact loess
11 soils and natural clays, with similar processes of destructuration under load leading to
12 the behavior of the intact soil converging with that of the reconstituted. However, there
13 have been relatively few attempts to identify comprehensively the effects of structure
14 in loess following the same types of techniques used for sedimentary clays (e.g. Burland,
15 1990; Cotecchia & Chandler, 2000) or sands (e.g. Cuccovillo & Coop, 1999).

16

17 Loess composition in China varies not only with location but also with depth and these
18 variations represent changing geological environments during the Quaternary,
19 especially changes to the nature, size or location of the source area and/or winds (Liu,
20 1985; Ding et al., 1997). While many researchers have also reported variations of
21 mechanical properties with depth (Liu, 1985) these studies have generally not
22 highlighted the role of structure and how that changes with depth. It is possible that the

1 broadly common origin of the soils might give rise to more similarity in the underlying
2 mechanical behavior if suitable normalization for the intrinsic properties were made.

3

4 The work described herein placed particular emphasis on investigating the influences
5 of structure and the interaction of structure with depth of burial in the context of the
6 macro-mechanical behavior of the soil in a saturated state. While the partial saturation
7 that is typical of loess in situ has important engineering consequences and interacts with
8 the effects of structure, a complete investigation of the saturated behavior is a necessary
9 first step to understanding the mechanics. Most loess research in China concentrates on
10 the silty loesses because of the collapse that they undergo during saturation, but here a
11 clayey loess has been tested that is not subject to collapse, but which will be shown
12 nevertheless to have a significant effect of structure on its behavior.

13 **MATERIALS AND PROCEDURES**

14 The samples tested were obtained from south Jingyang platform at depths below ground
15 level of 20m and 50m, both depths belonging to Middle Pleistocene (Q_2). The loess of
16 the Chinese plateau is normally consolidated (Shao et al., 2011), so these should be the
17 maximum depths of burial. Both soils were retrieved from areas cut for soil extraction
18 and although the locations were about 7km apart the ground levels of the plateau were
19 within about 2m of each other. A block sampling method was adopted clearing about
20 1m of superficial loess prior to excavation. The blocks were carefully trimmed by hand
21 and sealed using layers of cling-film (plastic wrap) and wax.

22

1 The index properties for the two materials are presented in Table 1. The dry density of
2 the shallower loess is 1500-1520kg/m³ with a void ratio of 0.81-0.83. The deeper loess
3 is significantly denser than the shallow, with a dry density of 1580-1590kg/m³ with a
4 void ratio of 0.72-0.74. Figure 2 shows the particle size distributions determined by
5 conventional sieving and sedimentation. The amount of silt in the two soils is similar at
6 about 75–77% but the deeper sample is slightly better graded over the silt size range.
7 The clay contents were the same for the two soils at about 18%. Mineralogical analysis
8 showed that the predominant mineral for the soil fraction is quartz, with smaller
9 amounts of albite and calcite with significant quantities of clay minerals (Table 2). Both
10 materials have relatively low plasticities but that at 50m is slightly higher, perhaps the
11 result of the small difference in grading or the slightly higher montmorillonite content.
12 Both materials plot slightly above the A-Line on the plasticity chart, and are classified
13 as CL, inorganic clays of low to medium plasticity, but are quite close to the ML region
14 for inorganic silts.

15

16 Figure 3 shows typical SEM images of the intact loess specimens for the two depths
17 tested, taken on broken horizontal and vertical surfaces. Many of the particles have a
18 platy shape and these tend to be more visible as flat surfaces in the horizontal plane
19 than the vertical, especially for the 20m sample, indicating a predominant horizontal
20 particle orientation, as might be expected. The particles also tend to be clustered into
21 aggregates, but at 20m the aggregate particles seem more loosely packed than those at
22 50m. Both samples have larger voids between the aggregates and these are also more

1 evident at 20m. The 20m sample therefore has a clearly more open texture. A higher
2 magnification image in Fig.3(e) shows an amorphous coating over many of the particles.
3 This was found at both depths, and while it could create some cement bonding between
4 particles it was local in nature not pervasive throughout the samples. The 50m block
5 sample had a homogenous meso-scale fabric at the scale visible to the naked eye, but
6 the 20m sample had a number of visible voids (Fig.4), probably of biogenic origin.

7

8 The intact triaxial samples were carefully trimmed vertically on a hand lathe to the
9 required dimensions of 38mm diameter and 76mm length, while the intact oedometer
10 samples were trimmed directly into the 50mm confining ring on the lathe applying some
11 downward pressure on the ring while trimming slightly ahead of the cutting edge. The
12 reconstituted samples for both triaxial and oedometer tests were made from the
13 trimmings and were created by the moist tamping method, taking care to use sufficient
14 compaction to avoid any macro-voids remaining and using the undercompaction
15 method of Ladd (1978).

16

17 Tables 3 and 4 give summary data for all the tests. For the oedometer tests the accuracy
18 of the initial specific volumes, $v (=1+e)$ was ensured by using two methods of
19 calculation, the first method measuring the initial dimensions and weights of the
20 samples and the second the water contents at the ends of the tests together with the
21 volumetric strains measured during testing. Any tests for which the differences between
22 the two values were more than ± 0.01 were discarded. An average value of v is reported

1 in Table 3 and these should therefore be accurate to better than ± 0.005 . The intact soil
2 was partially saturated with a degree of saturation typically of about 60% for the 20m
3 sample and 70% for the 50m. The reconstituted samples were also initially partially
4 saturated because of their creation by wet compaction. While the immersion in the water
5 bath was found sufficient to give good final saturation of the oedometer samples, the
6 triaxial samples were saturated under back pressure until B values of at least 95% were
7 achieved.

8

9 In the oedometer tests care was taken that the stresses applied to the intact samples
10 during saturation caused neither significant swelling or compression, to prevent
11 destructuration. The vertical stress was therefore varied to hold a constant height during
12 the initial stages of the test. The stresses required were quite low, at around 10kPa, but
13 as will be shown later, the swelling line gradients of the samples were small, so there
14 was not a strong tendency either to swell or compress at low stress levels. Similar initial
15 stresses were applied to the intact triaxial samples, because during saturation the true
16 volumetric strains are unknown, as the volumetric strain measured by the back pressure
17 volume gauge has a component arising from the dissolution and/or compression of air
18 within the sample. Since there was no local measurement of volume change on the
19 apparatus, the values of specific volume reported in Table 4 for the triaxial tests at the
20 end of saturation are based solely on the final water content measurements, together
21 with the volumetric strain during the test after saturation. The triaxial samples were all
22 isotropically compressed in small steps to a variety of stress levels and then sheared in

1 compression either undrained or drained.

2

3 **INFLUENCE OF STRUCTURE ON COMPRESSION BEHAVIOUR**

4 The one dimensional and isotropic compression data for reconstituted samples and
5 intact samples are plotted in Fig.5. The reconstituted samples were made with a variety
6 of initial specific volumes to check whether the various compression paths would
7 converge onto unique Intrinsic Compression Lines (ICL), or if there was any evidence
8 of transitional behavior with non-convergent compression curves (e.g. Altuhafi et al.,
9 2010; Shipton & Coop, 2012). With the exception of one isotropic test that may not
10 have been loaded quite far enough to reach the ICL, or may have some slight inaccuracy
11 in v , all the tests on reconstituted samples define unique ICLs in both isotropic and one-
12 dimensional loading. Although there are some small variations in the properties such as
13 grading and mineralogy, these seem not to affect the ICLs that are similar for both
14 depths.

15

16 The data for the two intact block samples both clearly reach states outside the ICLs, in
17 one-dimensional and isotropic loading which is an indication of the effects of structure.
18 These tests were started at relatively low effective stresses for two reasons, firstly so
19 that the pre-yield behavior could be observed in compression and secondly to avoid any
20 possible collapse that might have occurred had the samples been saturated at their in-
21 situ stress levels. At the original in-situ stresses the intact samples would have states
22 well outside the ICLs and so collapse could have been an issue.

1

2 The compression plots show that even for saturated loess the effects of structure can be
3 very significant and that although the geological origin is very different, the effects of
4 structure on compression are broadly similar in character and magnitude to those for
5 sedimentary clays (e.g. Cotecchia & Chandler, 2000; Hosseini Kamal et al., 2014). The
6 intact soil compression paths reach states to the right of the ICL and gross yield points
7 can be clearly identified as the points where the stress–volume behavior changes
8 significantly, after which the paths tend to converge with their respective ICLs for
9 isotropic or one-dimensional loading. The term “gross yield” is adopted as used in the
10 sensitivity framework of Cotecchia & Chandler (2000) because, as they pointed out the
11 strains below them are usually not purely elastic.

12

13 Burland (1990) proposed normalizing the compression data of intact clay samples
14 relative to the gradient and intercept of the reconstituted soil in order to highlight the
15 effects of structure to give void index, I_v :

16

$$17 \quad I_v = \frac{e - e_{100}^*}{e_{100}^* - e_{1000}^*} \quad (\text{Eq.1})$$

18

19 where e_{100}^* and e_{1000}^* are the void ratios on the ICL at 100 and 1000kPa. This method
20 was originally proposed for clays, but in Fig.6(a) it has been applied to these loess soils,
21 although the curvature of the ICL from Fig.5(a) is slightly smaller than for the
22 sedimentary clays analyzed by Burland. The data for the intact samples resemble those
23 of Feda et al. (1993) for a European loess that they also normalized using void index.

1

2 The history of suction in-situ is not known but the water table is well below the sample
3 depths (Lei, 2001; Xu et al., 2011). The gross yield points are quite close the estimated
4 past total stresses and so the effects of in-situ suction cannot have been large or those
5 yield stresses would have been increased under the combination of the total stress and
6 suction. The relatively stiff initial loading behavior and the small volumetric strains that
7 occur prior to reaching stress levels equal to the in-situ total stress are indications that
8 the samples were not badly disturbed either through sampling or laboratory preparation.

9

10 The gross yield points and possible in-situ maximum stresses both plot close to the
11 Sedimentation Compression Line (SCL) defined by Burland for the in-situ states of
12 normally consolidated clays. As Cotecchia & Chandler highlighted the SCL of Burland
13 corresponds to soils having a sensitivity of about 5 and since these samples yield at
14 slightly lower stresses, the sensitivities are moderate and slightly less than 5. In
15 comparison the swell sensitivity (Schmertmann, 1969), defined as the ratio of swelling
16 indices of the reconstituted and intact soils, C_{sr}/C_s , has values of about unity prior to
17 gross yield, and this does not change after yield. This would imply that there is no effect
18 of structure, which is unusual and seems not to agree with the clear yield in compression.

19

20 As highlighted by Coop & Cotecchia (1995) and Baudet & Stallebrass (2004) one key
21 difficulty of Burland's void index is that it is only defined in terms of vertical stress for
22 one dimensional compression and a new parameter v_n , was therefore defined in terms

1 of invariants, so that isotropic and one-dimensional compression data as well as
2 shearing data may all be compared:

3

$$4 \quad v_n = \exp\left(\frac{\ln(v) - N^*}{\lambda^*}\right) \quad (\text{Eq.2})$$

5

6 Figure 6(b) shows the volumetric compression data, normalized using v_n , for both the
7 natural and reconstituted loess. To allow for the curvature that Burland highlighted in
8 Intrinsic Compression Lines when examined over an extended pressure range and that
9 can be seen in the oedometer data in Fig.5(a), they are assumed to be straight when a
10 logarithmic specific volume axis is used, as suggested by Butterfield (1979):

11

$$12 \quad \ln v = N^* - \lambda^* \ln p' \quad (\text{Eq.3})$$

13 where values of 0.833 and 0.061 have been used for N^* and λ^* respectively. Although
14 the equations are defined in natural logs, \log_{10} scales are shown for convenience on
15 Fig.6(b). This method of normalization uses the isotropic normal compression line of
16 the reconstituted soil rather than the one dimensional as the reference condition and so
17 these data plot on the straight ICL, with a gradient of -1, with the one dimensional
18 compression data for the reconstituted plotting slightly below. In calculating p' for the
19 oedometer tests the simple assumption has been made that $K_0=1-\sin\phi'$. Over an
20 extended pressure range the isotropic and one-dimensional data diverge slightly and so
21 in choosing the gradient of the ICL the oedometer data, which cover a much greater
22 pressure range have been trusted more than the isotropic compression. This slight
23 difference in gradients may result from end friction in the triaxial tests, which had

1 conventional platens. Comparing the oedometer and isotropic compression tests for the
2 intact samples, the gross yield points are fairly similar, as are the rates of convergence
3 towards the ICL, indicating that destructuration occurs at fairly similar rates in one-
4 dimensional and isotropic loading for these soils.

5

6 The comparison of the data for the 20m and 50m samples gives an insight into the
7 evolution of structure with depth and so the origins of the structure, not previously
8 investigated for loess soils. The similarity of the intrinsic properties corresponds to
9 there being only relatively small differences in grading, mineralogy and index
10 properties, and indicates that the nature of the loess deposited at the two depths and
11 times was fairly similar. It also means that the comparison of the compression behavior
12 can be made equally well on either the normalized plots (Fig.6) or non-normalized
13 (Fig.5) since a key reason for normalization is to remove the effects of composition.

14 The two block samples have slightly different initial specific volumes, the deeper loess
15 having a slightly lower value as expected, but in both one-dimensional and isotropic
16 compression the gross yield points for the two depths are at quite similar distances
17 outside the ICL, and those in one-dimensional compression are close to the SCL. After
18 yield, the rates of convergence with the ICL are also similar for the two depths. These
19 similarities confirm that the soil has a predominantly sedimentation structure, as
20 defined by Cotecchia & Chandler (2000), so that the formation of the structure should
21 have been coincident with rather than subsequent to burial. The differences in in-situ
22 specific volume and yield stress are thus simply those expected from the different burial
23 depths. Sedimentation structure is typical of younger, normally or lightly
24 overconsolidated clays, as opposed to geologically older overconsolidated clays that
25 general possess some form of post-sedimentation structure formed after burial.

26

1 INFLUENCE OF STRUCTURE ON SHEARING BEHAVIOUR

2 Stress-Strain Behavior

3 Figure 7 presents typical stress-strain data for the intact and reconstituted samples; the
4 changes of pore pressures are normalized by initial effective confining pressure, p'_0 .

5 The initial states of each tests are on the isotropic ICL for the reconstituted samples and
6 above the ICL for the intact and so the volumetric strains and pore pressure responses
7 during shearing are compressive for both. Most of the tests were stopped at axial strains
8 of at least 40% at which point they had generally reached constant stress and volume
9 states, although there are some small continued changes for some of the intact samples.

10 The application of such large strains caused some barreling of the samples, although
11 the strongly contractive volume changes meant that this was less noticeable in the
12 drained tests.

13

14 The behavior of the intact soil is distinctly stiffer initially than the reconstituted for
15 similar stress levels, again with clear gross yield points similar to those seen in
16 compression at which points the stress-strain behavior softens significantly. These gross
17 yield points are present even if the initial state is slightly post-gross yield in
18 compression, for example at 400kPa Test 50m_UU01. At initial states further beyond
19 gross yield, for example at 650kPa test 50m_UD03 the gross yield point during shearing
20 is absent. For drained conditions the intact soil continues to strain harden after gross
21 yield while for undrained it strain softens rapidly, a feature that is not seen for the
22 reconstituted soil and might again be attributed to the effects of structure.

1

2 In Fig.8 the stress-strain data are represented by a stress ratio, q'/p' . Again the intact
3 samples can be seen to be stiffer for similar loading conditions, but it is also clear that
4 while the 20m samples tend towards a final ratio M of 1.35 those from 50m have a
5 lower final value of around 1.25, most tests being within about ± 0.05 of these values.
6 These values of M correspond to critical state angles of shearing resistance, ϕ'_{cs} of 33.4°
7 and 31.1° respectively. The lower M at 50m depth is consistent with the slightly higher
8 plasticity.

9

10 **Stress-Dilatancy Behavior**

11 The stress-dilatancy relationships for the drained tests on the reconstituted loess from
12 20m in Fig.9(a) give a straight relationship at larger strains. In the absence of elastic
13 shear and bulk moduli, total strains have been plotted, the shear strain being calculated
14 as $\varepsilon_s = \varepsilon_v - \varepsilon_a/3$, which assumes isotropy. The gradients have been taken by regression
15 over short sections of the $\varepsilon_s : \varepsilon_v$ graph. There is some scatter in the data at low stress
16 ratios, because the rate of dilation is calculated as the ratio of two small values of strain.
17 When the data for the intact samples from 20m are compared with the reconstituted
18 (Figs.9b) the relationships are significantly different, reflecting the influence of the
19 natural structure. At small strains the paths initially reach higher stress ratios than the
20 equivalent reconstituted soil, but then tend towards the same critical state M at large
21 strains. For the 50m depth the data are a little less clear, and there is little significant
22 difference between the intact and reconstituted samples. The tendency towards the

1 lower M value of 1.25 seen in Fig.8 occurs relatively late in some tests. There was no
2 clear visual evidence of strain localization so this is unlikely to be the cause.

3

4 **Critical States**

5 In Fig.10 the undrained stress paths highlight the differences between the intact and
6 reconstituted samples that indicate effects of structure, with the intact samples giving
7 stress paths that are significantly more strain softening. The end of test states have been
8 assumed to be critical states and these again confirm the different M values.

9

10 For consistency with the v_n graph the shearing paths are shown in the $\ln v : \ln p'$ plane in
11 Fig.11. The paths followed by many of the intact samples are more strongly
12 compressive, with greater volume changes for the drained tests and higher pore
13 pressures for the undrained since they start with higher initial specific volumes. Zhou
14 et al. (2014) also highlighted the strongly strain-softening behavior of an intact loess
15 that resulted from initial states far above the critical state line, which they attributed to
16 structure, but they could not confirm this as they did not make comparisons with
17 reconstituted soils. Even if the paths for the intact samples indicate a strongly
18 compressive behavior, the end of test states give a critical state line (CSL) that lies
19 higher than that of the reconstituted samples.

20

21 The CSLs for both reconstituted and intact samples (CSL_r and CSL_i) are the same for
22 the two depths in either the $\ln v : \ln p'$ plane or $\ln v_n : \ln p'$ plane (Fig.12) and in the

1 normalized plane they are parallel to the ICL. It is perhaps surprising that the relatively
2 small differences in the grading and index properties of the soil at the two depths has
3 some effect on the critical states in the stress plane, $q':p'$ but not in the compression
4 plane $\ln v:\ln p'$, but this is consistent with there being no effect also on either the isotropic
5 or one-dimensional intrinsic compression behavior.

6

7 The spacing between the CSLs for the intact and reconstituted soil in terms of specific
8 volume is around 0.08, which would represent a volumetric strain of about 5% for the
9 initial specific volumes of the samples. Although there is some very small continued
10 volume change at the end of the tests for some of the drained tests on intact samples
11 (Fig.7c) it is clear that incomplete testing could not be the cause of there being two
12 different CSLs. Provided that a soil has a homogenous structure, shearing should
13 eventually lead to a unique critical state when all elements of the initial structure are
14 erased and the soil should tend towards not only constant stresses and volumes, but also
15 a constant fabric. However, Nougier-Lehon et al. (2005) demonstrated that the strains
16 needed to reach a constant fabric could be very large indeed. Many models for
17 structured soils assume ultimate convergence of the intact with the reconstituted states
18 (e.g. Liu et al., 2013). In contrast, to account for more stable elements of fabric that
19 could not be removed by the strain levels imposed by triaxial testing, in their framework
20 Cotecchia & Chandler (2000) assumed that the CSL of the intact soil need not
21 correspond with that of the reconstituted. This was implemented in their constitutive
22 model by Baudet & Stallebrass (2004) by permitting an offset between the CSLs of the

1 intact and reconstituted soil, so that as an intact soil destructures it need not collapse
2 back to the CSL of the reconstituted soil, no matter what strains are applied. For clays
3 several examples have been observed where robust fabrics could not be broken down
4 by triaxial shearing, requiring the definition of different CSLs for intact and
5 reconstituted soils (Rampello & Silvestri, 1993; Coop & Cotecchia, 1995; Fearon &
6 Coop, 2000).

7
8 This lack of convergence of critical states during shearing contrasts with the better
9 convergence of the oedometer tests on Figs.5 and 6, although close inspection shows
10 that at higher pressures the critical states for the intact and reconstituted soils do plot
11 slightly closer together, perhaps the start of some convergence of the CSLs. The more
12 evident convergence of the oedometer test data may be the result of the much larger
13 stress levels applied and larger volumetric strains. In many constitutive models for
14 structured soils the volumetric strains are assumed to play a greater role in the
15 breakdown of the structure than the shear strains (e.g. Callisto et al., 2002), while in
16 some the destructureation is solely related to volumetric strains (e.g. Lagioia & Nova,
17 1995; Baudet and Ho, 2004).

18
19 Figure 13 shows SEM images of the intact and reconstituted soils from 20m after
20 triaxial shearing. The intact sample (Fig.13a and b) has a much denser fabric than before
21 shearing (Fig.3a and b) as a result of the strong volumetric compression it has
22 experienced. There is still the evident preferential orientation of the particles in the

1 horizontal plane and areas of the amorphous coating, possibly cementing, could still be
2 found (Fig.13c). The reconstituted soil was sheared drained at 400kPa while the intact
3 was sheared drained at 450kPa. Nevertheless the reconstituted soil seems still to have
4 a denser fabric than the intact as might be expected from the lower specific volumes at
5 critical state (Fig.13d and e). The difference between the horizontal and vertical
6 surfaces is also less evident and areas of possible cementing were less easily identified.

7

8 **Normalized Boundary Surfaces**

9 In Fig.14 the stress paths have been normalized for volume by an equivalent pressure
10 taken on the CSL, p'_{cs} , defined as:

11

$$12 \quad p'_{cs} = \exp\left(\frac{\Gamma^* - \ln V}{\lambda^*}\right) \quad (\text{Eq.4})$$

13

14 where λ^* and Γ^* are the gradient of the CSL and its intercept at intercept at 1 kPa in the
15 $\ln v : \ln p'$ plane. To reduce some small scatter of the normalized paths when identifying
16 the state boundary surfaces, it has been assumed that any slight difference in the final
17 specific volume and that on the chosen CSL (either intrinsic or intact) in Fig.11 arises
18 from small inaccuracies in specific volume and so the final values have been adjusted
19 to lie on those lines. Because of the two different M values for the two depths, the values
20 of q/p'_{cs} have been further divided by M so that the CSL plots at 1,1.

21

22 The paths for the reconstituted soil in Fig.14a define a clear reconstituted or intrinsic

1 state boundary surface (SBS_r). The shape of this intrinsic surface shares more similarity
2 with those of sands (e.g. Coop & Lee, 1993) than those of clays (e.g. Hosseini-Kamal
3 et al., 2014), since the spacing between the isotropic ICL and the CSL_r is relatively large
4 at about 2.6 when expressed as a ratio of stresses, and the CSL_r lies to the left of an
5 apex of the boundary surface (i.e. a maximum value of q'/Mp'_{cs}). The normalized paths
6 of the undrained tests tend also to plot inside the boundary surface defined by the
7 drained tests, so that Rendulic's principle is not obeyed. In sands, Coop & Lee (1993)
8 attributed these features to particle breakage but none could be detected in these tests
9 and similar behavior has been found in gap graded residual soils by Ferreira & Bica
10 (2006) also without breakage.

11

12 In Fig.14b the stress paths of the tests on intact samples have been normalized with
13 respect to the CSL_i . These are compared with the intrinsic SBS_r normalized with respect
14 to the CSL_r , i.e. two different CSLs are assumed. The differences between undrained
15 and drained tests are much accentuated with the normalized drained tests for low to
16 medium stress levels reaching large stress ratios before a gross yield is seen after which
17 the path drops rapidly back towards the critical state, a feature that can also be seen in
18 the $\ln v : \ln p'$ plane (Fig.11). The sizes of the intact state boundary surfaces (SBS_i) are
19 both considerably larger than the SBS_r , again indicating the effects of structure. Once
20 isotropic compression prior to shearing takes the initial state past the gross yield, the
21 normalized stress paths tend to collapse back towards the SBS_r , giving the paths that
22 are more rounded with gross yield at lower stress ratios, converging with the shape of

1 the SBSr. This behavior is again similar to cemented sands (e.g. Cuccovillo & Coop,
2 1999) or structured clays (Cotecchia & Chandler, 2000). Figure 14(c) compares the two
3 boundary surfaces when they are both normalized with respect to the intrinsic critical
4 state line, emphasizing the separation of the two surfaces in volumetric space.

5

6 Comparing the two depths, the intrinsic behavior demonstrated by the normalized stress
7 paths of the reconstituted samples (Fig.14a) is again very similar, apart from the
8 different M values. For the intact samples the SBS_i have similar shapes, but the larger
9 SBS_i for the 20m samples tends to indicate a stronger effect of structure at this depth.

10 This can also be seen the isotropic gross yield points in Fig.6(b) which is slightly further
11 outside the ICL for the 20m depth than for 50m. However, as Hosseini-Kamal et al.
12 (2014) and Gasparre & Coop (2008) have emphasized, apparently larger effects of
13 structure at shallower depths and higher initial specific volumes can be an artefact of
14 this type of volumetric normalization. Older and/or more deeply buried clays, with
15 lower in-situ I_v (or v_n) values, reach states that are not as far outside the ICL as clays
16 with higher initial I_v , but this is generally unrelated to the relative effects of structure in
17 shearing.

18

19 **CONCLUSIONS**

20 An investigation was made of the effects of structure in a clayey loess from the Chinese
21 Jingyang platform has been carried out, comparing two depths within a stratum of loess
22 that has a similar geological age and origin and reasonably homogenous composition.

1 The deeper loess had a lower in situ specific volume and was slightly more plastic, but
2 otherwise the effects of structure on the larger strain behavior were quite similar, the
3 shallower loess generally having a slightly greater effect of structure. The intact
4 structure of the soil caused stiffer initial behavior in shearing, defining gross yield
5 points that could be seen in both compression and shearing that marked the onset of
6 destructuration. Although of a very different genesis, and having a low plasticity, the
7 behavior of the loess could be analyzed within the same framework as is commonly
8 used for sedimentary clays and the effects of structure were broadly similar to those in
9 clays of medium sensitivity. Some elements of structure were relatively robust and
10 could not be easily broken down unless loaded to very large stress levels in the
11 oedometer. At the low to medium stress levels used in the triaxial tests two different
12 critical state lines could be defined from the end of test states, with little evidence of
13 their convergence with continued shear strain. This was confirmed qualitatively by
14 observations of the persistence of differences of fabric and possibly some bonding after
15 shearing.

16

17 **ACKNOWLEDGEMENTS**

18 The work was supported by the Natural Science Foundation of China (Project No.
19 51109199) and the Hong Kong Scholars Program. The first author would like to express
20 his sincere thanks to Dr. Fanyu Zhang of Lanzhou University for his help in some
21 laboratory testing on loess index properties, and Prof. Sun Jimin of the Institute of
22 Geology and Geophysics, Chinese Academy of Sciences for his help in drawing the
23 map of loess distribution.

24

1 NOMENCLATURE

2		
3	C_s	swelling index of intact soil
4	C_{sr}	swelling index of reconstituted soil
5	e	voids ratio
6	I_v	void index (Eq.1)
7	K_0	coefficient of earth pressure
8	N^*	intercept at 1kPa of isotropic ICL in $\ln v : \ln p'$ plane (Eq.3)
9	p'	mean normal effective stress
10	p'_{cs}	equivalent value of p' taken on CSL (Eq.4)
11	p'_0	mean normal effective stress at start of shearing
12	q	deviatoric stress
13	u	pore pressure
14	v	specific volume ($=e+1$)
15	v_n	normalized specific volume (Eq.2)
16	Γ^*	intercept of the CSL at 1kPa in $\ln v : \ln p'$ plane
17	λ	gradient of ICL or CSL in $v : \ln p'$ plane
18	λ^*	gradient of ICL or CSL in $\ln v : \ln p'$ plane (Eq.3)
19	σ'_v	vertical effective stress in oedometer
20	CSL	critical state line
21	ICL	isotropic intrinsic compression line
22	SCL	sedimentation compression line

25 REFERENCES

- 26
- 27 Altuhafi F., Baudet B.A. & Sammonds P. (2010). The mechanics of subglacial sediment:
28 an example of new “transitional behaviour”. Canadian Geotechnical Journal 47(7): 775-
29 790.
- 30 Barden L., McGown A. & Collins K. (1973). The collapse mechanism in partly
31 saturated soil. Eng. Geol., 7, 49-60.
- 32 Baudet, B.A. & Ho, E.W.L. (2004). On the behaviour of deep-ocean sediments.
33 Géotechnique, 54(9), 571-580.
- 34 Baudet, B. & Stallebrass, S. (2004). A constitutive model for structured clays.
35 Géotechnique, 54(4), 269-278.
- 36 Burland, J.B. (1990). On the compressibility and shear strength of natural soils.
37 Géotechnique 40(3), 329-378.
- 38 Butterfield, R. (1979). A natural compression law for soils (an advance on $e - \log p'$).
39 Géotechnique, 26(4), 469-480.
- 40 Callisto, L, Gajo, A, & Wood, D.M. (2002). Simulation of triaxial and true triaxial tests
41 on natural and reconstituted Pisa clay. Géotechnique, 52(9), 649-666.
- 42 Chen, C., Zhu, Z. & Gao, P. (2006). Research on relationship between structure and
43 deformation property of intact loess. Rock and Soil Mechanics, 27(11), 1892-1896.

1 Coop, M.R. & Cotecchia, F. (1995). The compression of sediments at the
2 archaeological site of Sibari. Proc. 11th ECSMFE, Copenhagen, 8, 19-26.

3 Coop, M.R. & Lee, I.K. (1993). The Behaviour of Granular Soils at Elevated Stresses.
4 In "Predictive Soil Mechanics" Houlsby, G.T. & Schofield, A.N. eds. (Thomas Telford,
5 London) (Proc.C.P.Wroth Memorial Symposium, 1992), 186-198.

6 Cotecchia, F. & Chandler, R.J. (2000). A general framework for the mechanical
7 behaviour of clay. *Géotechnique* 50(4), 431-447.

8 Cuccovillo, T. & Coop, M.R. (1999). On the mechanics of structured sands.
9 *Géotechnique*, 49(6), 741-760.

10 Delage, P., Cui, Y.J. & Antoine, P. (2005). Geotechnical problems related with loess
11 deposits in Northern France. Proc. Int. Conf. on Problematic Soils, Eastern
12 Mediterranean University, Famagusta, N. Cyprus, 1-24.

13 Derbyshire E., Meng X., Wang J., Zhou Z. & Li B. (1995). Collapsible loess on the
14 loess plateau of China. In *Genesis and Properties of Collapsible Soils*, E. Derbyshire et
15 al. eds, Kluwer Academic Publishers. 267-293.

16 Dijkstra, T.A. (2001). Geotechnical thresholds in the Lanzhou loess of China.
17 *Quaternary International*, 76/77, 21-28.

18 Dijkstra, T.A., Rappange, F.E., van Asch, T.W.J., Li, Y.J. & Li, B.X. (2000).
19 Laboratory and in situ shear strength parameters of Lanzhou loess. In: Derbyshire, E.,
20 Meng, X.M., Dijkstra, T.A. (Eds.), *Landslides in the Thick Loess of North-West China*,
21 Chapter 5. Wiley, Chichester, 131-172.

22 Ding, Z., Sun, J., Rutter, N.W., Rokosh, D. & Liu, T. (1997). Changes in Sand Content
23 of Loess Deposits along a North-South Transect of the Chinese Loess Plateau and the
24 Implications for Desert Variations. *Quaternary Research*, 52, 56-62.

25 Fearon, R.E. & Coop, M.R. (2000). Reconstitution: what makes an appropriate
26 reference material? *Géotechnique*, 50(4), 471-477.

27 Feda, J., Bohac, J. & Herle, I. (1993). Compression of collapsed loess: Studies on
28 bonded and unbonded soils. *Eng. Geol.*, 34, 95-103.

29 Ferreira, P.M.V. & Bica, A.V.D. (2006). Problems in identifying the effects of structure
30 and critical state in a soil with a transitional behavior. *Géotechnique* 56(7), 445-454.

31 Gasparre, A. & Coop, M. R. (2008). The quantification of the effects of structure on the
32 compression of a stiff clay. *Canadian Geotech. J.* 45(9), 1324-1334.

33 Heller, F. & Liu, T.S. (1982). Magnetostratigraphical dating of loess deposits in China
34 *Nature*. Vol. 300, 431-433.

35 Hosseini-Kamal, R., Coop, M.R. & Jardine, R.J. & Brosse, A. (2014). The post-yield
36 behaviour of four Eocene-to-Jurassic UK stiff clays. *Géotechnique*, 64(8), 620-634.

37 Hu, Z., Shen Z. & Xie, D. (2004). Deformation properties of structural loess. *Chinese*
38 *J. Rock Mechs & Eng.*, 23(24), 4143-4145.

39 Jiang, M., Hu, H. & Liu, F. (2012). Summary of collapsible behaviour of artificially
40 structured loess in oedometer and triaxial wetting tests. *Can. Geotech. J.* 49, 1147-1157.

41 Jiang, M.J., Zhang, F.G., Hu, H.J., Cui, Y.J., Peng, J.B. (2014). Structural
42 characterization of natural loess and remolded loess under triaxial tests. *Eng. Geol.*, 181,
43 249-260.

- 1 Kukla, G. & An, Z. (1989). Loess stratigraphy in Central China. *Palaeogeography,*
2 *Palaeoclimatology, Palaeoecology*, 72, 203-225.
- 3 Ladd, R. S. (1978). Preparing test specimens using under-compaction. *Geotech. Testing*
4 *J.*, 1(1), 16-23.
- 5 Lagioia, R. & Nova, R. (1995). An experimental and theoretical study of the behaviour
6 of a calcarenite in triaxial compression. *Géotechnique*, 45(4), 633-648.
- 7 Lei, X. Y. (2001). *The Geo-Hazards and Human Activities on Chinese Loess Platform:*
8 *The Geological Publishing House, Beijing, 244 pp.*
- 9 Li, J. & Yao, Y. (2009). Critical state model of Ko consolidated structure loess. *J. Xi'an*
10 *Univ. Arch. & Tech. (Natural Science Edition)*, 42(4), 533-537.
- 11 Liu, T.S. (Ed.) (1985). *Loess and the Environment.* Science Press, Beijing, 215 pp.
- 12 Liu, M. D., Liu, J., Horpibulsuk, S. & Huang, W. (2013). Simulating the stress and
13 strain behavior of loess via SCC model. In C. Leung, S. Goh & R. Shen (Eds.), 18th
14 Southeast Asian Geotechnical Conference: Geotechnical Infrastructure. Singapore:
15 Research Publishing. 455-460.
- 16 Muñoz-Castelblanco, J., Delage, P., Pereira, J.M. & Cui, Y.J. (2011) Some aspects of
17 the compression and collapse behaviour of an unsaturated natural loess. *Géotechnique*
18 *Letters*, 1(2), 17-22.
- 19 Nougier-Lehon, C., Vincens, E. & Cambou, B. (2005). Structural changes in granular
20 materials: the case of irregular polygonal particles. *Intl. J. Solids and Structures*, 42 (24-
21 25), 6356-6375.
- 22 Rampello, S. & Silvestri, F. (1993). The stress-strain behaviour of natural and
23 reconstituted samples of two overconsolidated clays. In *Geotechnical engineering of*
24 *hard soils soft rocks* (eds A. Anagnostopoulos et al.), Rotterdam: Balkema. 769-778.
- 25 Rogers, C.D.F., Dijkstra, T.A. & Smalley, I.J. (1994). Hydroconsolidation and
26 subsidence of loess: Studies from China, Russia, North America and Europe. *Eng. Geol.*,
27 37(2), 83-113.
- 28 Schmertmann, J. H. (1969). Swell sensitivity. *Géotechnique* 19(4), 530-533.
- 29 Shao, S., Luo, A., Yu, Q. & Zhou F. (2006). Structural damage properties of Q₃ loess
30 under triaxial loading and moistening. *Chinese J. Geotech. Eng.*, 28(12), 2078-2081.
- 31 Shao, S., Tao, H. & Xu, P. (2011) Discussion on research of mechanical characteristics
32 of loess considering structural behavior and its application. *Rock and Soil Mechanics*,
33 32, Supp.2, 42-50.
- 34 Shipton, B. & Coop, M.R. (2012) On the compression behaviour of reconstituted soils.
35 *Soils & Foundations*, 52(4), 668-681.
- 36 Wen, B-P. & Yan, Y-J. (2013). Influence of structure on shear characteristics of the
37 unsaturated loess in Lanzhou, China. *Eng. Geol.*, 168, 46-58.
- 38 Xu, L., Dai, F., Tham, L.G., Tu, X. & Jin, Y. (2011). Landslides in the Transitional
39 Slopes between a Loess Platform and River Terrace, Northwest China. *Environmental*
40 *& Engineering Geoscience*, 17(3), 267-279.
- 41 Zhou, Y.F., Tham, L.G., Yan, W.M., Dai, F.C. & Xu, L. (2014). Laboratory study on
42 soil behavior in loess slope subjected to infiltration. *Eng. Geol.*, 183, 31-38.

43
44

1 **List of table**

2

3 Table 1. Geotechnical index properties of the materials

4

5 Table 2. X-ray diffraction analyses of the materials

6

7 Table 3. Details of oedometer tests

8

9 Table 4. Details of the triaxial tests

10

11

12 **List of figure**

13

14 Fig.1. Sample location of Jingyang on the south Chinese Loess Plateau

15

16 Fig.2. Particle size distributions of the loess samples

17

18 Fig.3. SEM images of the intact micro-structure of the loess(a) 20m deep loess,
19 horizontal plane; (b) 20m deep loess, vertical plane; (c) 50m deep loess, horizontal
20 plane; (d) 50m deep loess, vertical plane; (e) Higher magnification image showing
21 coating over the particles (50m horizontal plane)

22

23 Fig.4. Photograph showing the meso-structure of the 20m loess

24

25 Fig.5. Compression curves of reconstituted and intact samples: (a) oedometer tests; (b)
26 isotropic compression curves from triaxial tests

27

28 Fig.6. Normalized compression data for natural and reconstituted loess (a) using void
29 index, I_v ; (b) normalized specific volume, v_n

30

31 Fig.7. Typical triaxial test data (a) deviator stress-axial strain curves, (b) pore pressure
32 responses for undrained tests (c) volume changes for drained tests. (R*** reconstituted,
33 U*** undisturbed, *D** drained, *U** undrained)

34

35 Fig.8. Development of stress ratio for reconstituted and undisturbed specimens

36

37 Fig.9. Stress-dilatancy data for the drained tests on (a) reconstituted specimens (20m);
38 (b) undisturbed specimens (20m); (c) reconstituted and undisturbed specimens (50m)

39

40 Fig.10. Stress paths for intact and reconstituted samples (a) entire range of stresses; (b)
41 enlargement for stresses less than 600kPa

42

43 Fig.11. Critical states line in the volumetric plane

44

1 Fig.12. Critical states line in the normalized volumetric plane

2

3 Fig.13. SEM images of samples after testing (a) 20m intact sample (No. 20m_UD03)
4 horizontal surface; (b) 20m intact sample (No. 20m_UD03) vertical surface; (c) 20m
5 intact sample (No. 20m_UD03) showing detail of coating over particles; (d) 20m
6 reconstituted sample (No. 20m_RD03) horizontal surface; (e) 20m reconstituted sample
7 (No. 20m_RD03) vertical surface

8

9 Fig.14. Normalized stress-paths of intact and reconstituted loess(a) Stress-paths of
10 reconstituted samples normalized by p'_{cs} using the intrinsic *CSL*; (b) Stress-paths of
11 intact samples normalized by p'_{cs} using intact *CSL*; (c) Stress-paths of intact samples
12 normalized by p'_{cs} using intrinsic *CSL*

13

1 Table 1. Geotechnical index properties of the materials

2

Sample	Initial void ratio	Intact dry density [kg/m ³]	Specific gravity	Liquid limit	Plastic limit	Plasticity index
JY-20m	0.81-0.83	1500-1520	2.73	28.3	17.1	11.2
JY-50m	0.72-0.74	1580-1590	2.74	35.6	18.5	17.1

3

4

1 Table 2. X-ray diffraction analyses of the materials

2

Sample	Quartz	Albite	Calcite	Dolomite	Montmorillonite	Illite	Kaolinite	Chlorite	Others
JY-20m	35.1%	14.9%	16.5%	2.3%	4.4%	15.5%	3.2%	6.1%	2.0%
JY-50m	32.3%	10.2%	19.0%	2.1%	7.4%	17.7%	3.5%	6.7%	1.1%

3

4

1 Table 3. Details of oedometer tests

Test number	Sample depth	Sample style	Method of sample preparation	Water content	Initial specific volume, v_0	σ'_{vmax} : MPa
O1	20m	Undisturbed	—	—	1.822	7.167
O2	50m	Undisturbed	—	—	1.710	7.167
O3	20m	Reconstituted	Slurry	—	2.331	1.098
O4	20m	Reconstituted	Wet compaction	10%	1.963	7.167
O5	20m	Reconstituted	Wet compaction	10%	1.797	7.167
O6	50m	Reconstituted	Slurry	—	2.151	1.103
O8	50m	Reconstituted	Wet compaction	10%	2.303	7.167

2

3

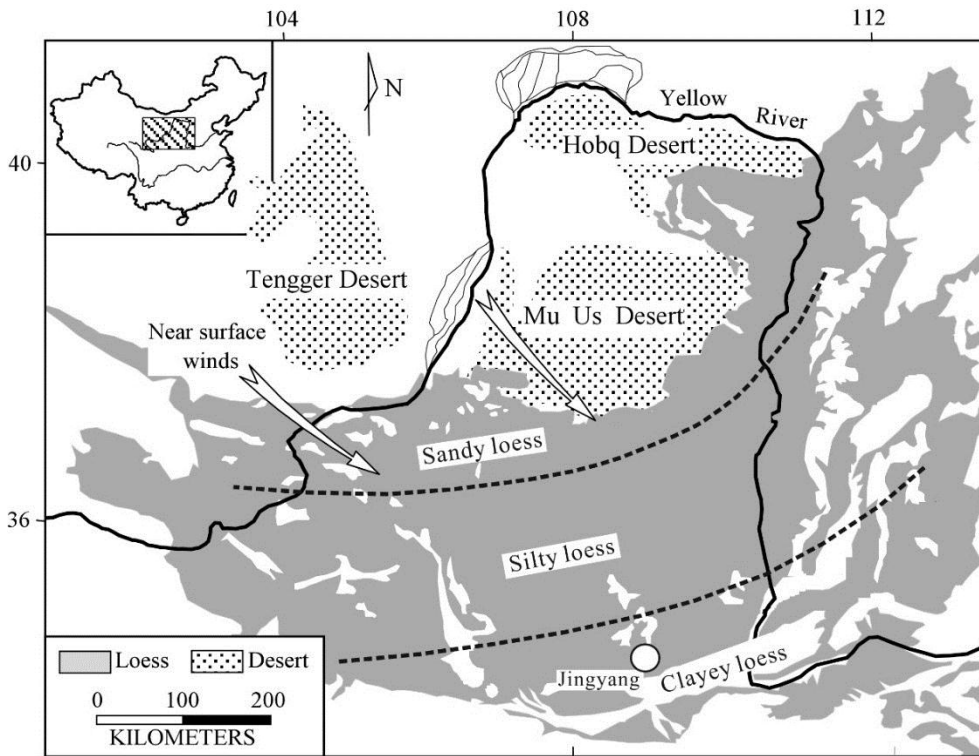
1 Table 4. Details of the triaxial tests

Test name	Sample types	Shearing types	Specific volume after saturation	Mean effective stress for shearing /kPa	Ends of test		
					Deviator stress: q_{cs} /kPa	Mean effective stress: p'_{cs} /kPa	Specific volume: v_f
20m_UD01	U	ICD	1.869	100	225.9	172.8	1.661
20m_UD02	U	ICD	1.872	200	454.8	350.1	1.612
20m_UD03	U	ICD	1.877	450	1126.3	826.3	1.508
20m_UU01	U	ICU	1.885	50	52.8	36.6	1.835
20m_UU02	U	ICU	1.834	300	80.3	56.6	1.774
50m_UD01	U	ICD	1.772	200	419.0	336.7	1.617
50m_UD02	U	ICD	1.778	420	811.0	687.0	1.574
50m_UD03	U	ICD	1.755	650	1348.5	1092.3	1.500
50m_UU01	U	ICU	1.783	400	169.3	128.8	1.726
20m_RD01	R	ICD	1.941	120	294.5	218.9	1.585
20m_RD02	R	ICD	1.864	250	579.1	440.6	1.514
20m_RD03	R	ICD	1.918	400	1000.1	733.9	1.483
20m_RD04	R	ICD	1.564	300	675.7	522.7	1.468
20m_RD05 (ORC=4)	R	ICD	1.892	100	233.3	179.1	1.589
20m_RU01	R	ICU	1.972	100	39.1	30.3	1.748
20m_RU02	R	ICU	1.698	200	131.1	99.9	1.630
20m_RU03	R	ICU	1.695	100	94.1	70.9	1.653
20m_RU04	R	ICU	1.906	300	137.2	104.3	1.643
50m_RD01	R	ICD	1.879	100	209.0	170.3	1.607
50m_RD02	R	ICD	1.901	300	710.5	541.2	1.479
50m_RD03	R	ICD	1.936	500	1227.0	981.6	1.448
50m_RU01	R	ICU	1.722	400	302.2	243.3	1.566
50m_RU02	R	ICU	1.936	600	381.5	292.6	1.555

2 Note: the test name, for example 20m_UD01, indicates the sample was 20m deep from the ground surface; ICD is
3 isotropically consolidated drained shearing; ICU is isotropically undrained shearing; “U” is undisturbed sample and
4 “R” is the reconstituted sample; the method of sample preparation for all reconstituted samples is wet compaction
5 with water content of about 10%.

6
7

1



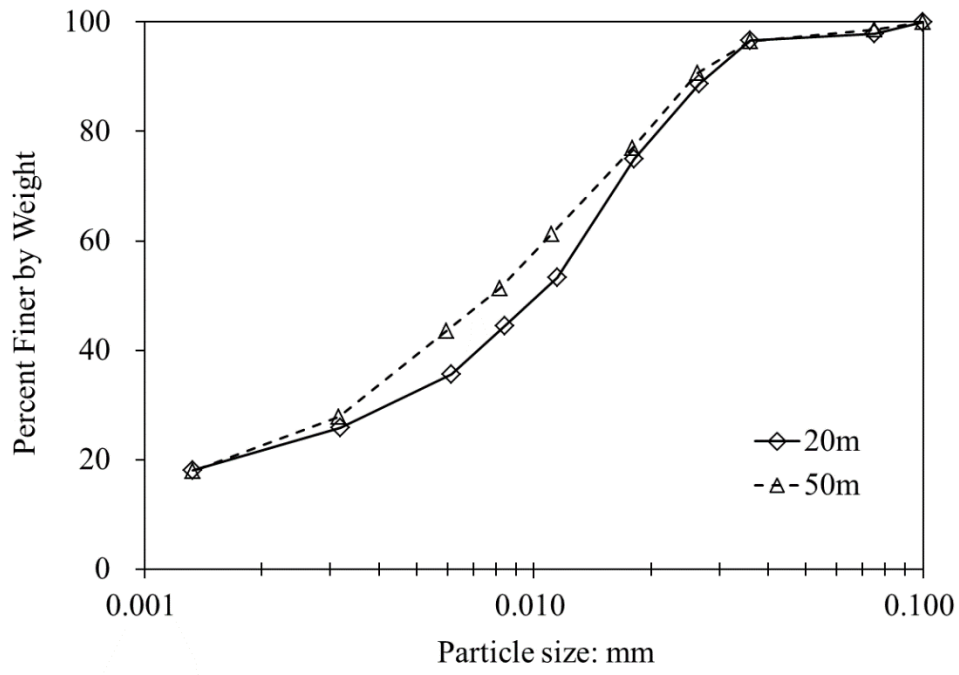
2

3

4

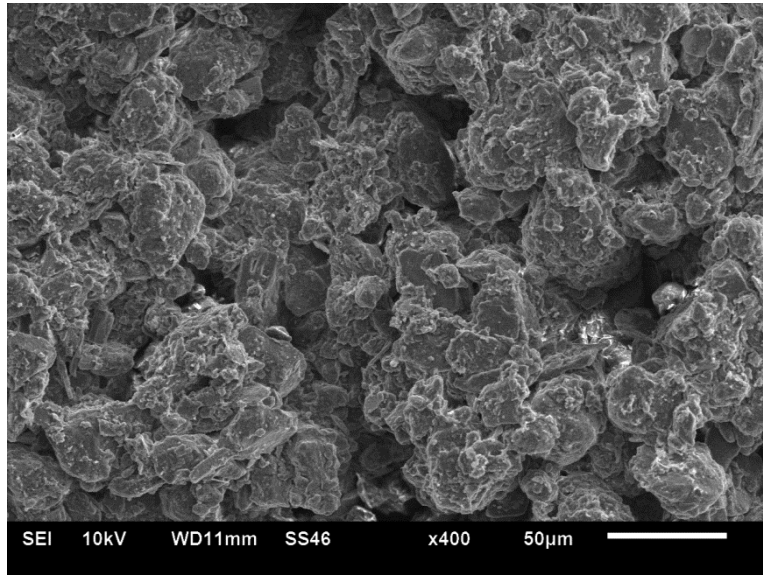
Fig. 1. Sample location of Jingyang on the south Chinese Loess Plateau

5



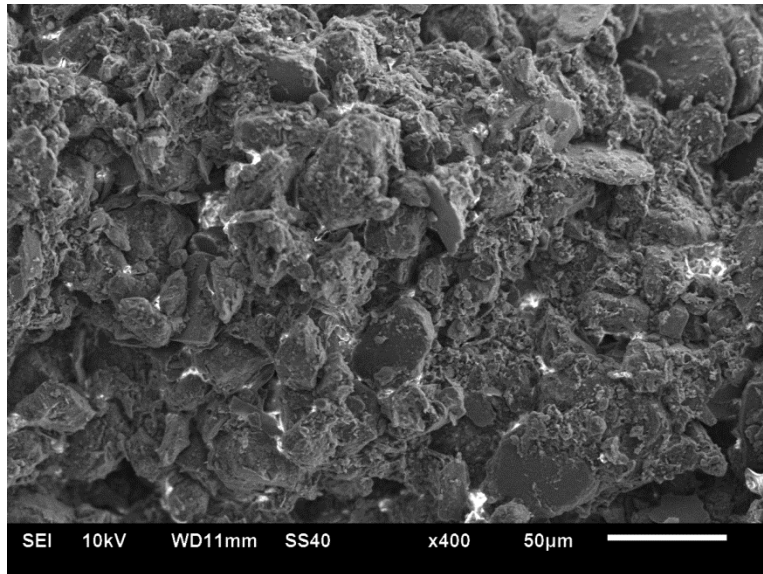
1
2
3
4

Fig. 2. Particle size distributions of the loess samples



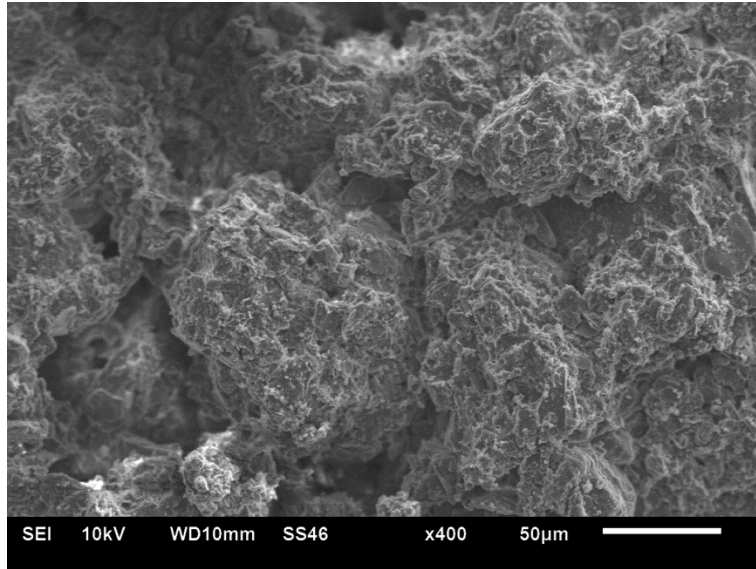
1
2
3
4

(a) 20m deep loess, horizontal plane



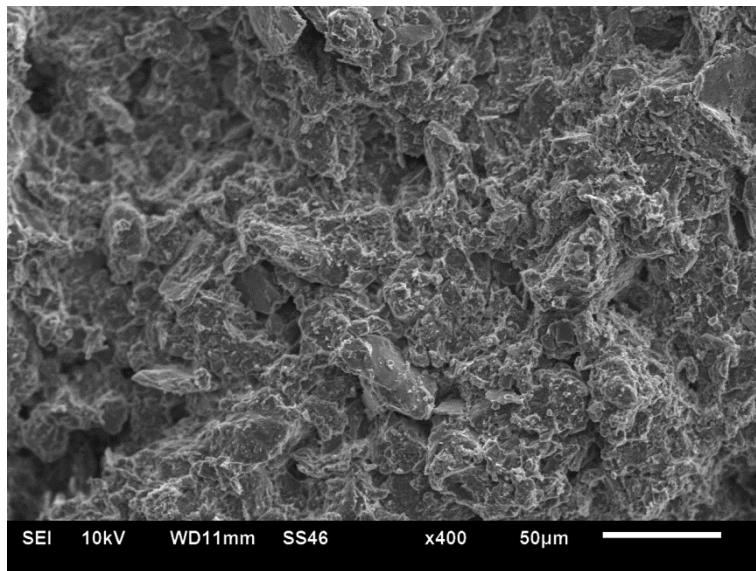
5
6
7
8

(b) 20m deep loess, vertical plane



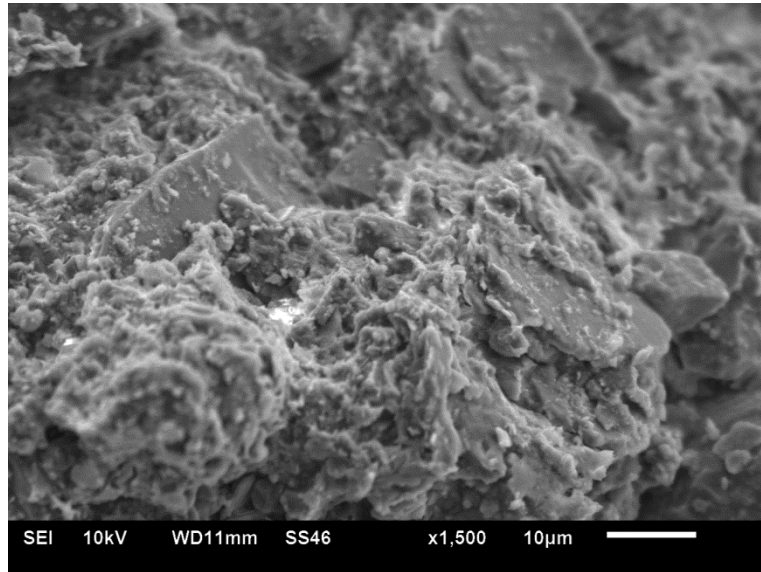
1
2
3
4

(c) 50m deep loess, horizontal plane



5
6
7
8

(d) 50m deep loess, vertical plane



1
2
3
4
5
6
7
8

(e) Higher magnification image showing coating over the particles (50m horizontal plane)

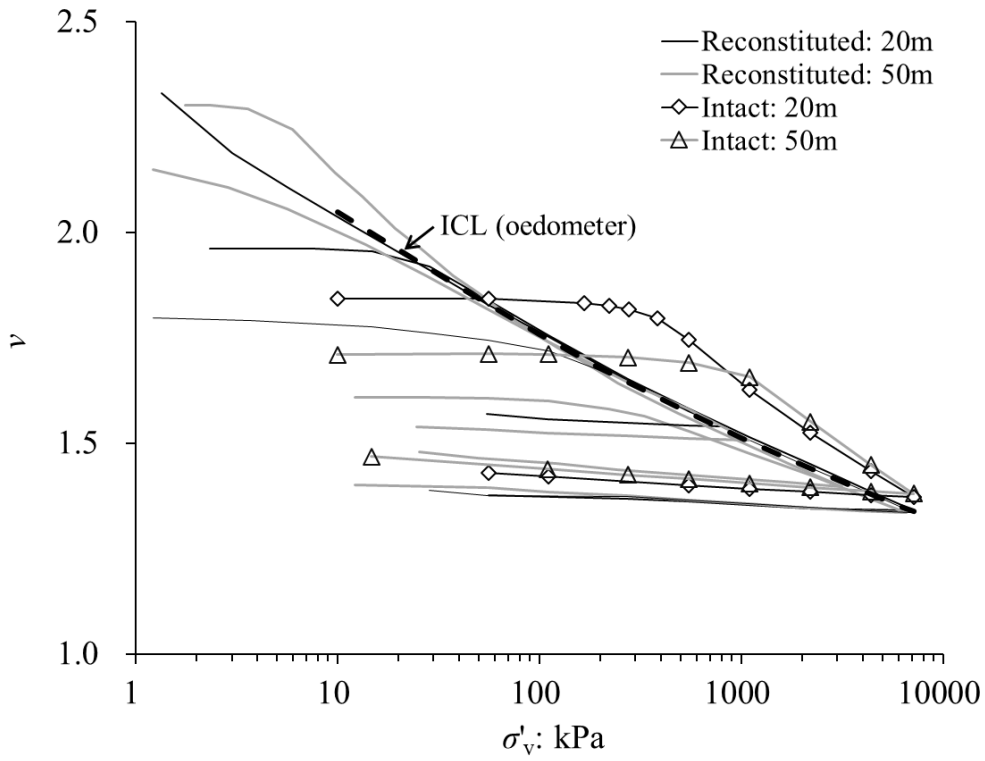
Fig.3. SEM images of the intact micro-structure of the loess



1
2
3
4

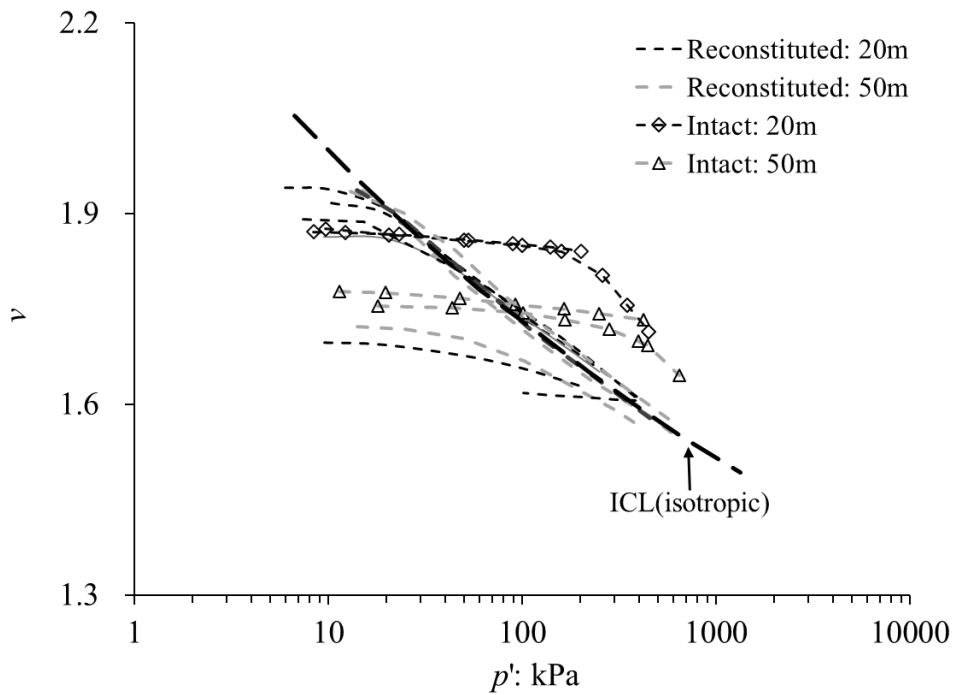
Fig.4. Photograph showing the meso-structure of the 20m loess

1



2

3 (a)



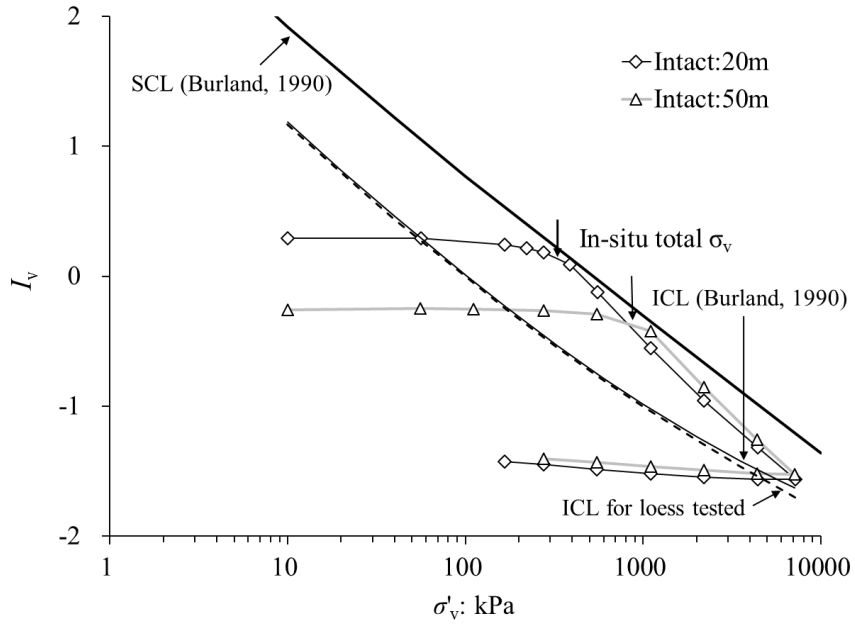
4

5

6 (b)

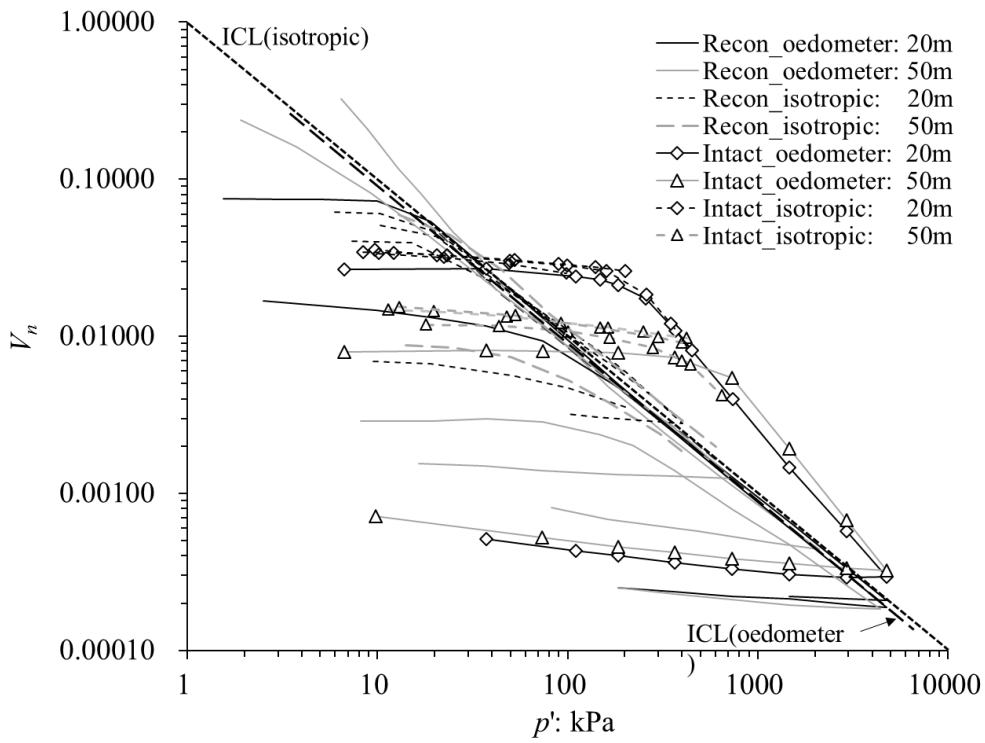
7 Fig. 5. Compression curves of reconstituted and intact samples: (a) oedometer tests; (b)
8 isotropic compression curves from triaxial tests

9



1
2
3

(a)



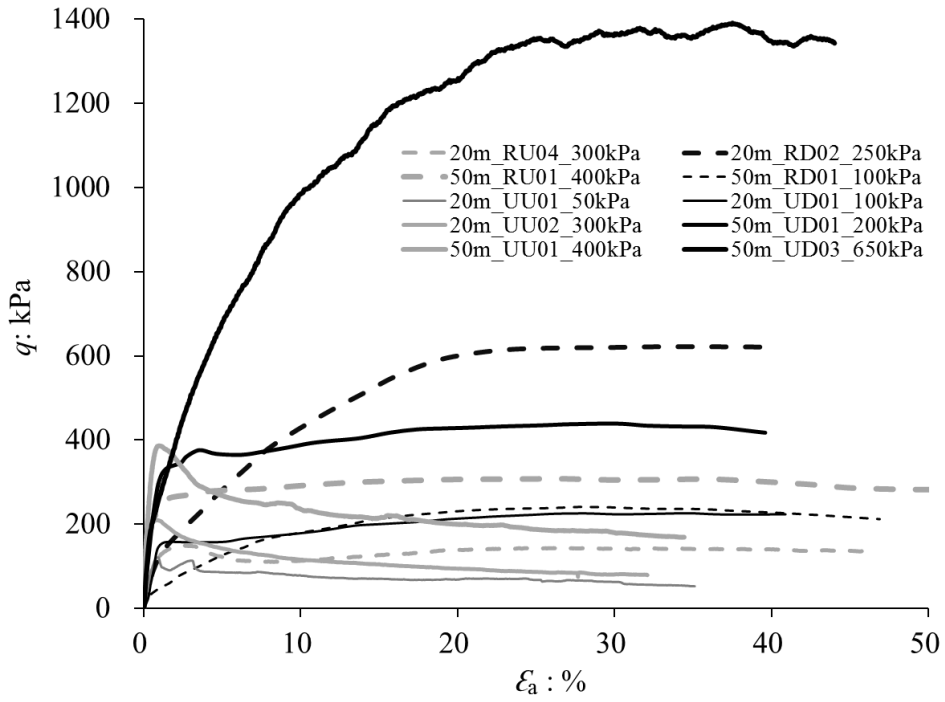
4
5

(b)

6 Fig. 6. Normalized compression data for natural and reconstituted loess (a) using void
7 index, I_v ; (b) normalized specific volume, v_n

8

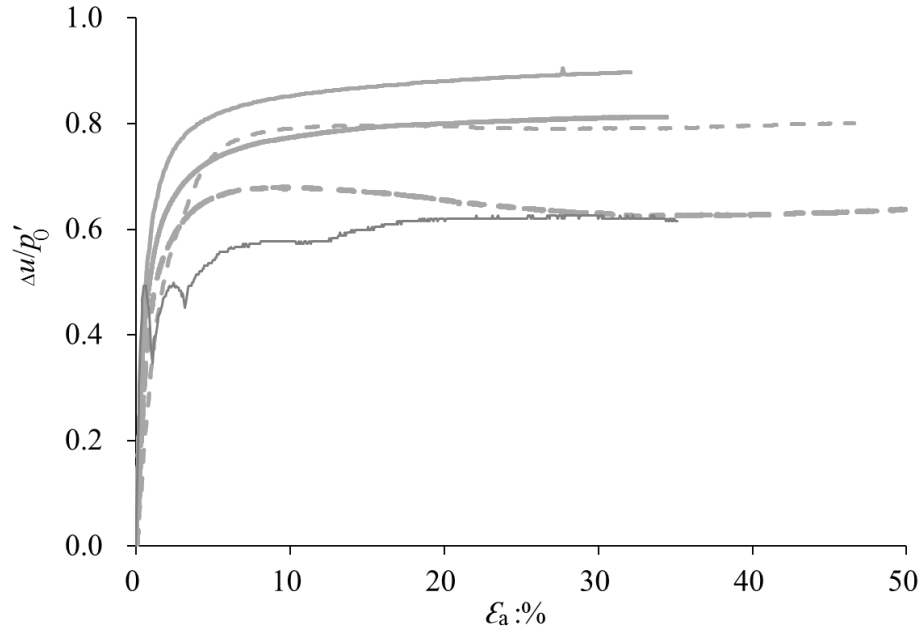
1



2

3

4 (a)

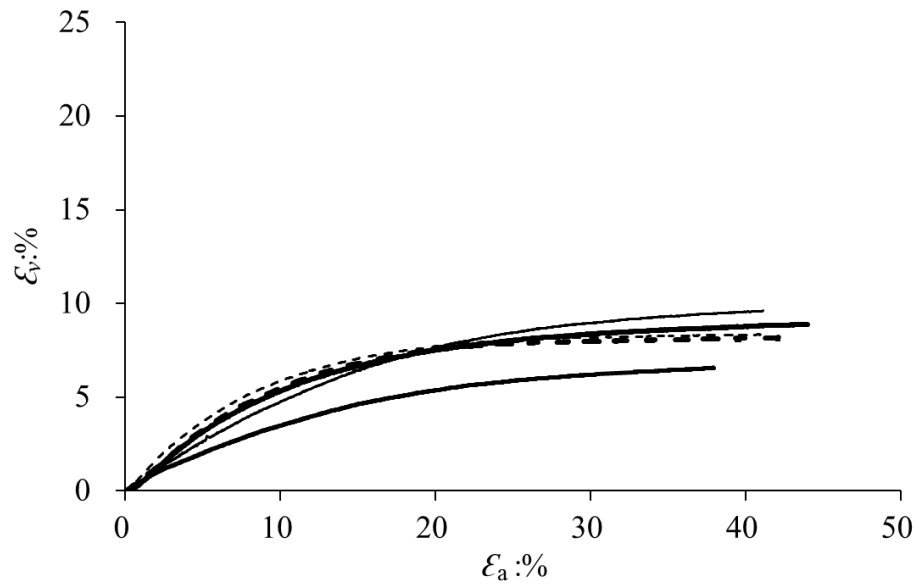


5

6 (b)

7

8

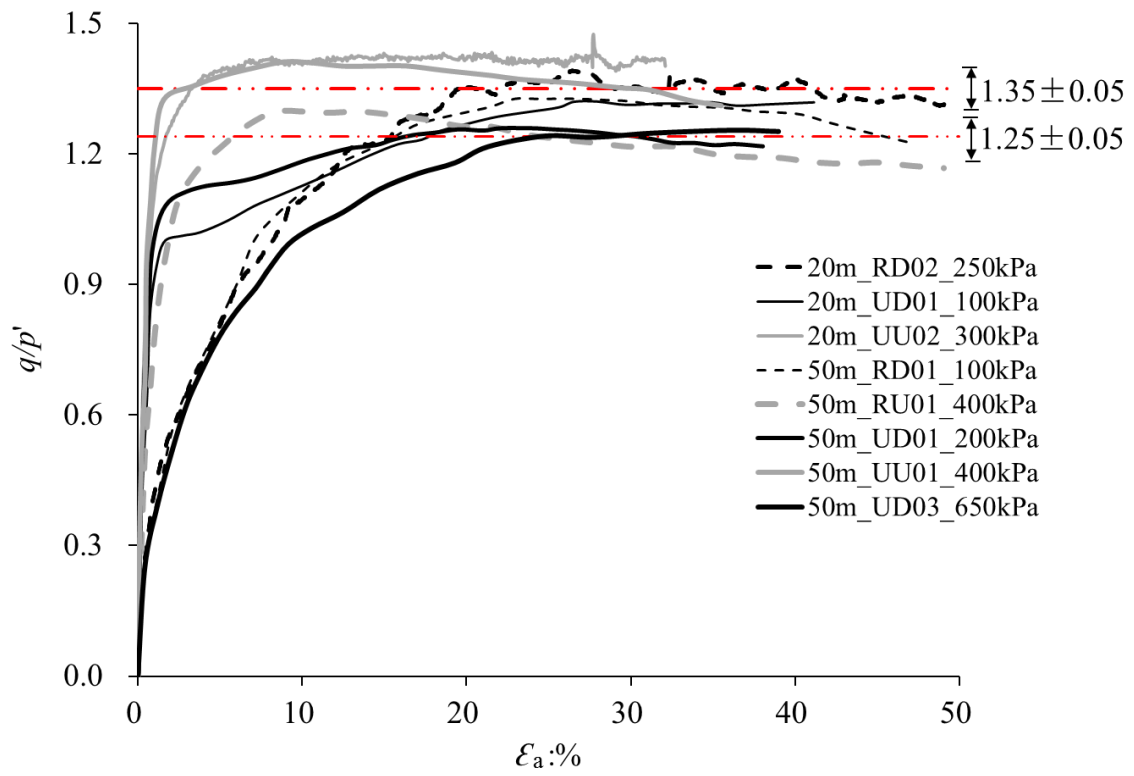


1
2
3
4
5
6
7
8

(c)

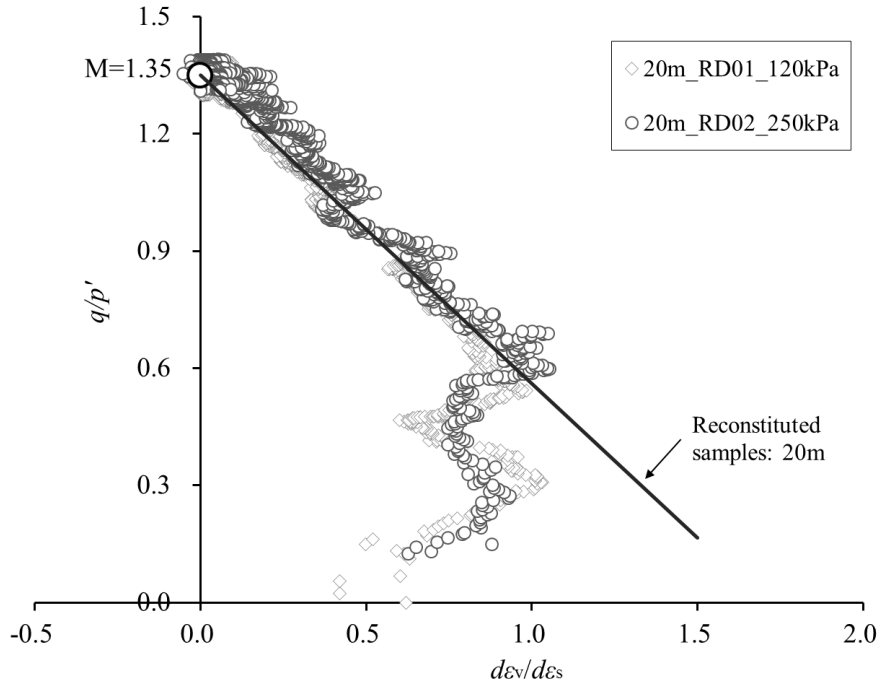
Fig.7. Typical triaxial test data (a) deviator stress-axial strain curves, (b) pore pressure responses for undrained tests (c) volume changes for drained tests. (R*** reconstituted, U*** undisturbed, *D** drained, *U** undrained)

1
2
3

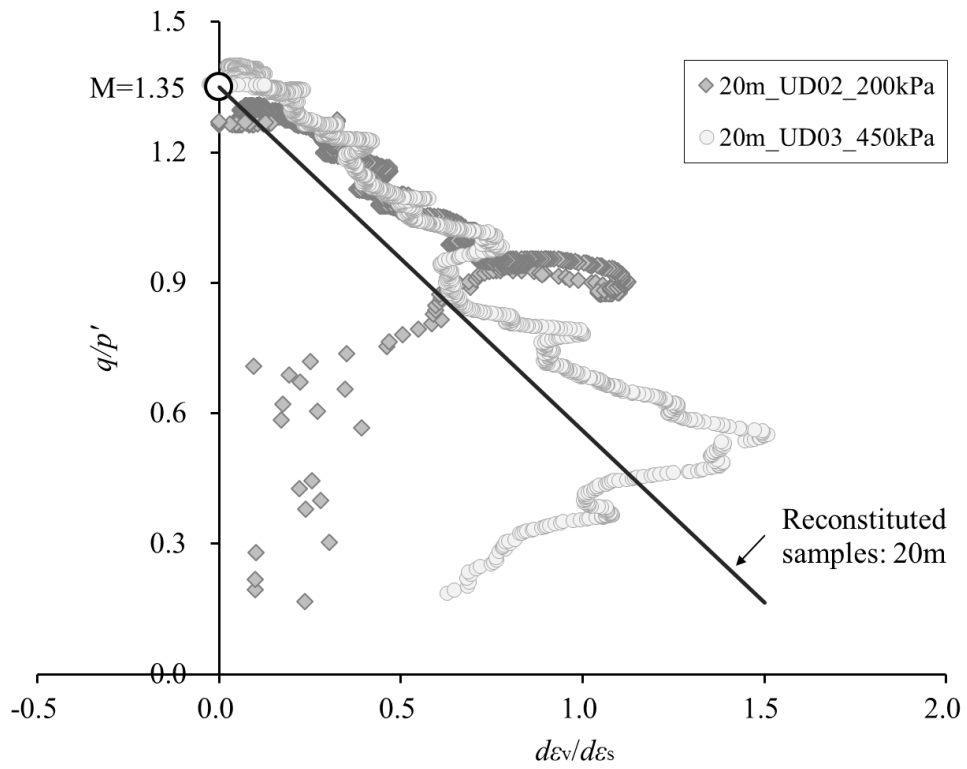


4
5
6
7
8
9

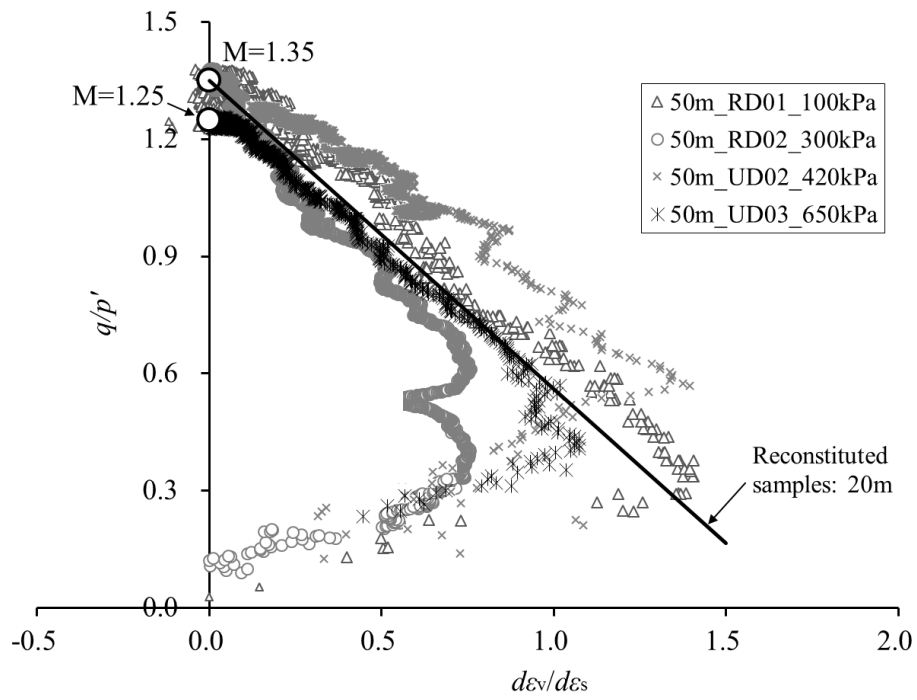
Fig.8. Development of stress ratio for reconstituted and undisturbed specimens



1
2 (a)



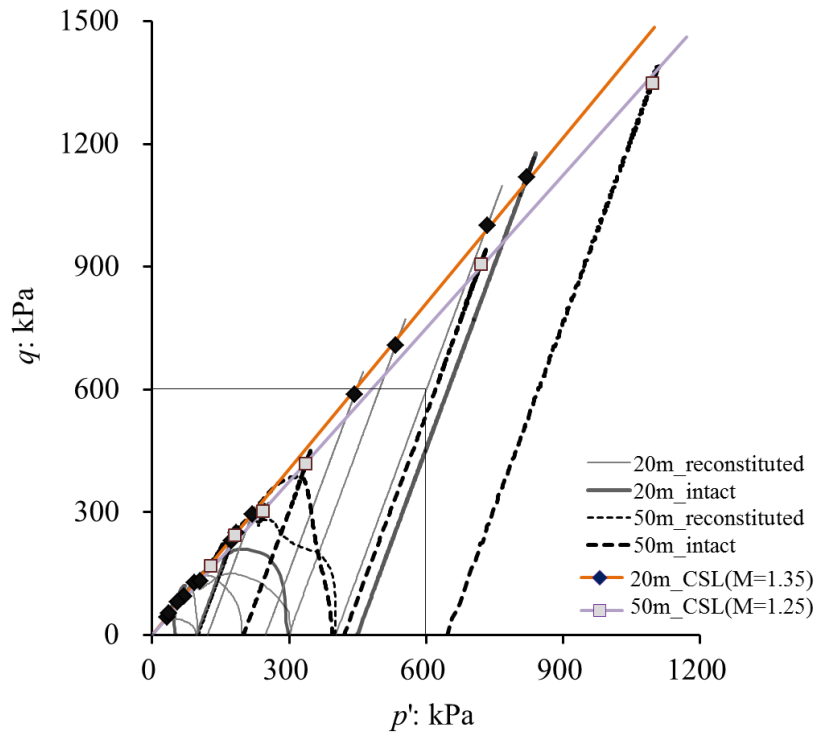
3
4 (b)
5
6



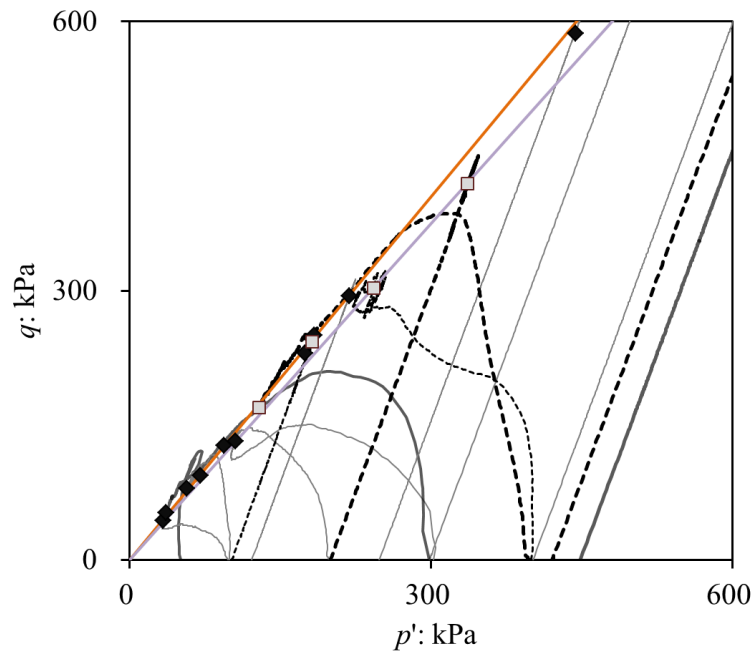
1
2
3
4
5
6
7
8

(c)

Fig.9. Stress-dilatancy data for the drained tests on (a) reconstituted specimens (20m);
 (b) undisturbed specimens (20m); (c) reconstituted and undisturbed specimens (50m)



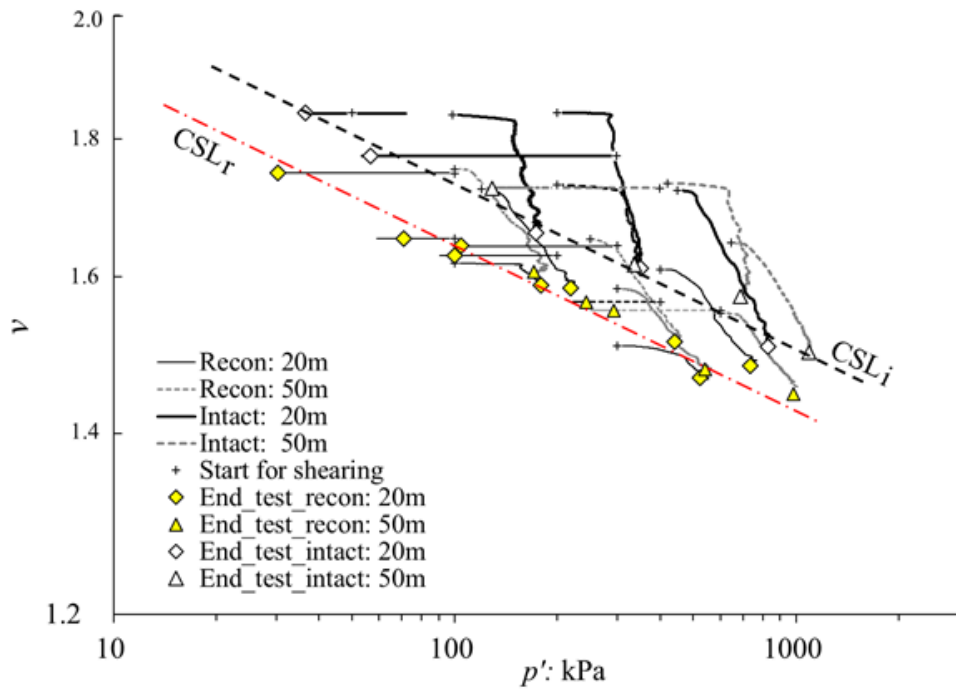
1
2 (a)



3
4 (b)

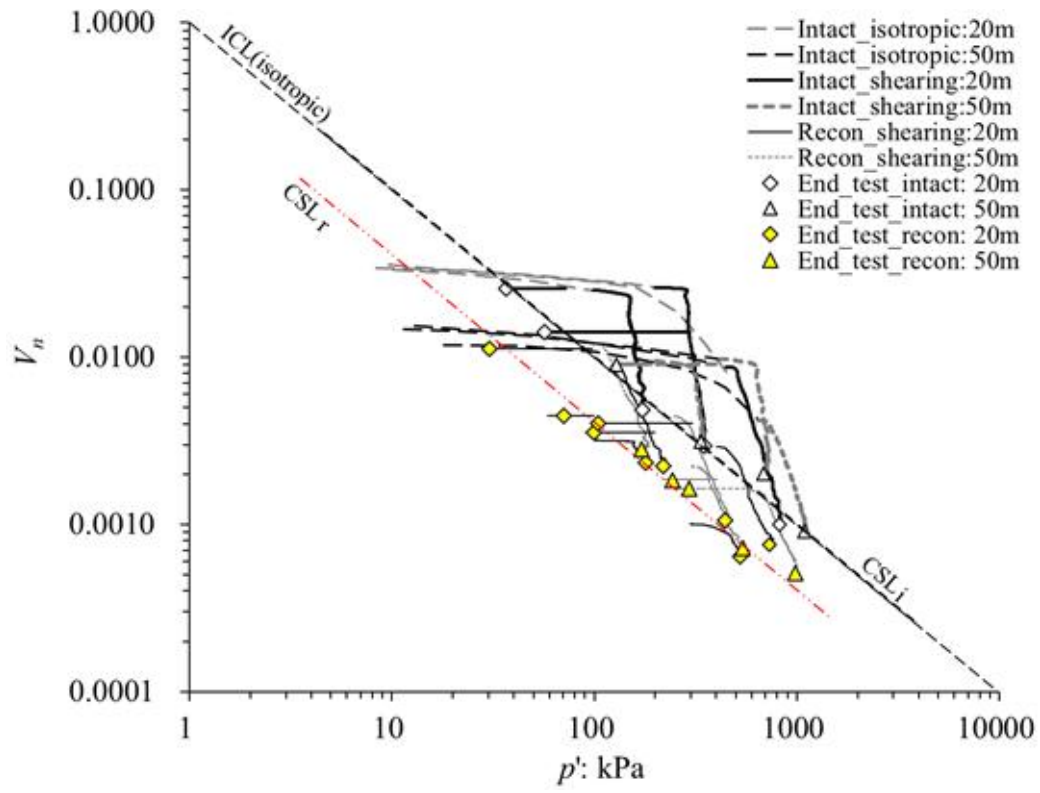
5 Fig.10. Stress paths for intact and reconstituted samples (a) entire range of stresses; (b)
6 enlargement for stresses less than 600kPa

7
8



1
2
3
4
5

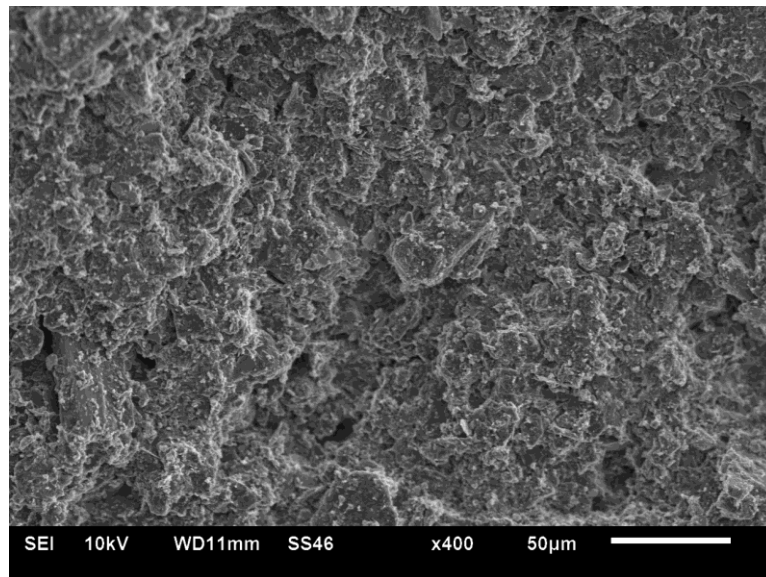
Fig. 11. Critical states line in the volumetric plane



1
2
3
4
5

Fig. 12. Critical states line in the normalized volumetric plane.

1



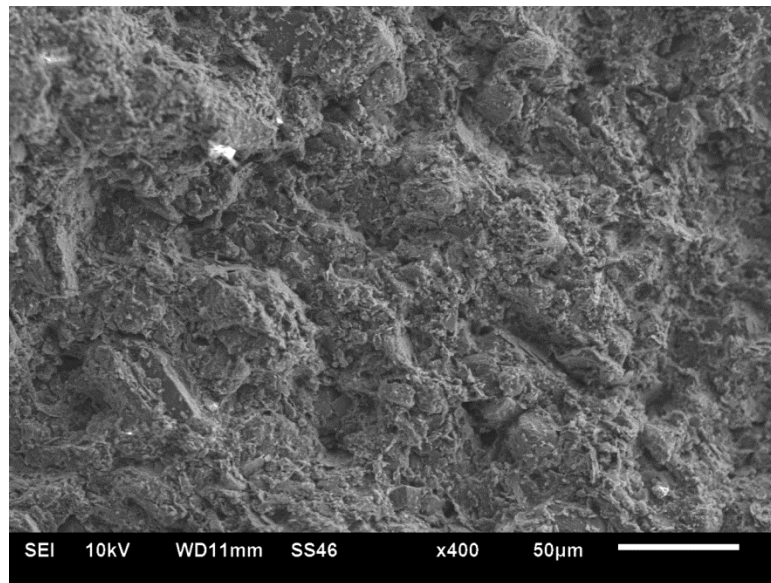
2

3

4

(a) 20m intact sample (No. 20m_UD03) horizontal surface

5



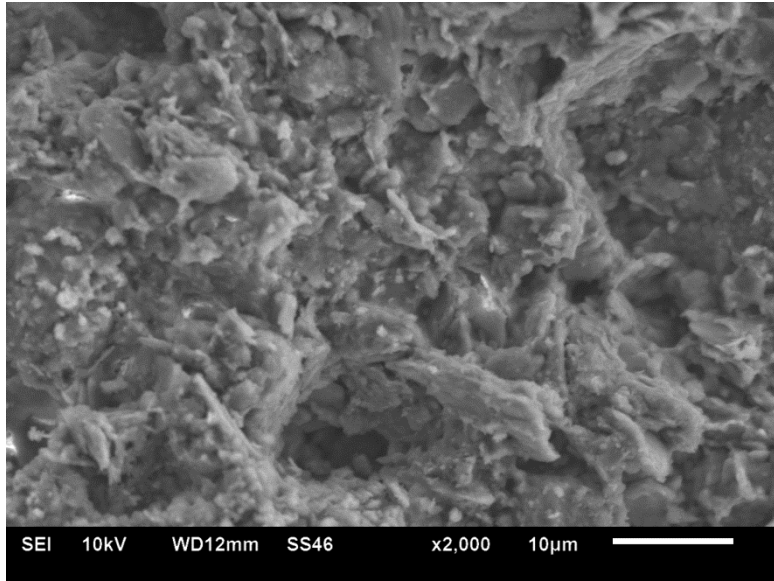
6

7

8

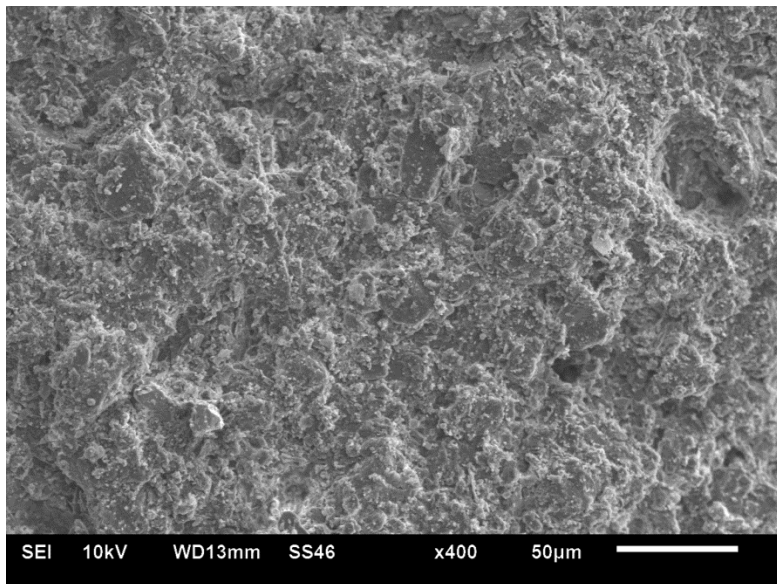
(b) 20m intact sample (No. 20m_UD03) vertical surface

9



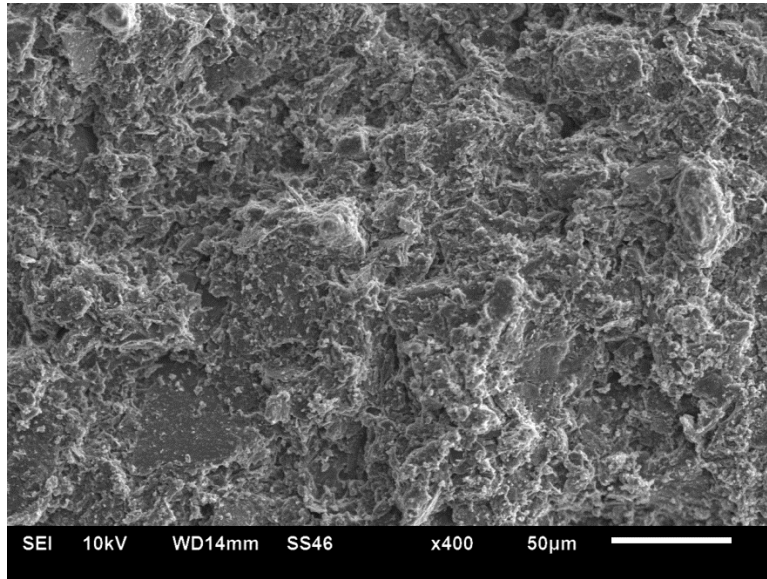
1
2
3
4

(c) 20m intact sample (No. 20m_UD03) showing detail of coating over particles



5
6
7
8

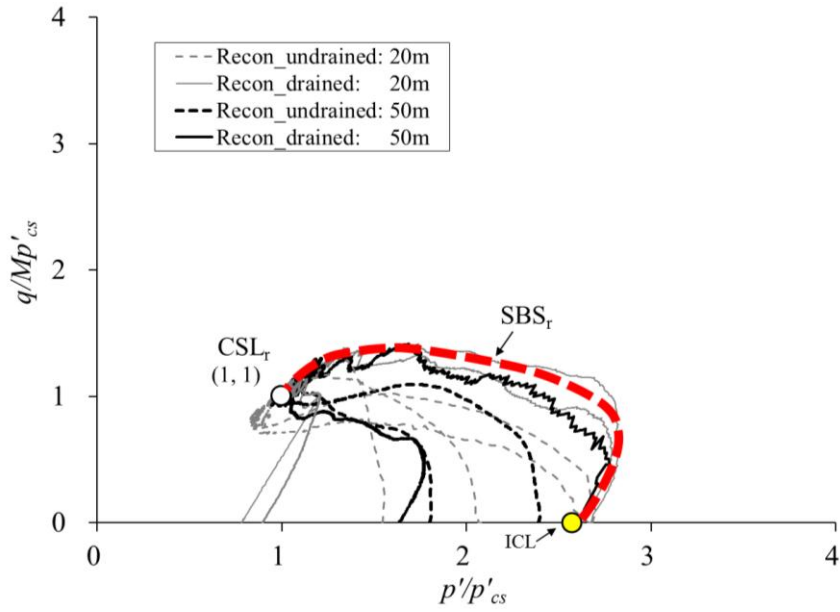
(d) 20m reconstituted sample (No. 20m_RD03) horizontal surface



1
2
3
4
5
6

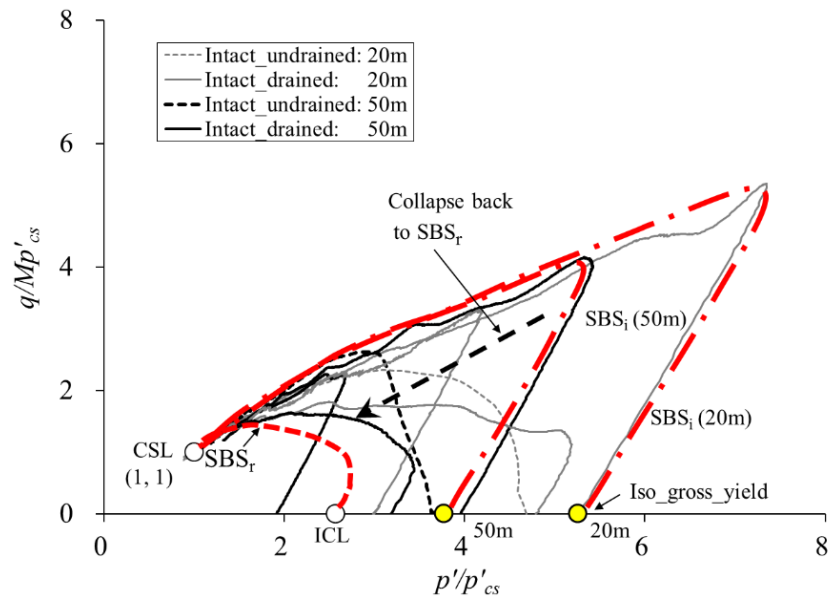
(e) 20m reconstituted sample (No. 20m_RD03) vertical surface

Fig.13. SEM images of samples after testing



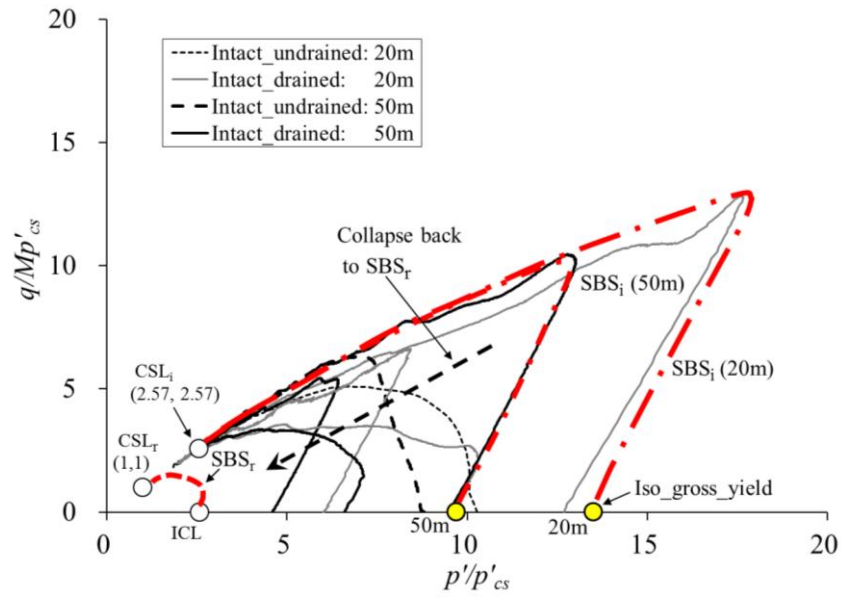
1
2
3
4
5

(a) Stress-paths of reconstituted samples normalized by p'_{cs} using the intrinsic CSL



6
7
8
9
10

(b) Stress-paths of intact samples normalized by p'_{cs} using intact CSL



1
2
3
4
5
6
7
8

(c) Stress-paths of intact samples normalized by p'_{cs} using intrinsic CSL

Fig.14. Normalized stress-paths of intact and reconstituted loess